Internal hydraulic jumps in two-layer flows with increasing upstream shear

Kelly A. Ogden[1] and Karl Helfrich[2]
[1]*Department of Mechanical and Materials Engineering, Western University, London, Ontario, Canada, N6A 5B9*
[2]*Department of Physical Oceanography, Woods Hole Oceanographic Institution, Woods Hole, Massachusetts 02541, USA*

(Received 16 October 2018; accepted 22 June 2020; published 21 July 2020)

Basic two-layer shock-joining theories for internal hydraulic jumps in flows with upstream shear do not have solutions when the shear becomes large. These theories conserve momentum flux and layer volume flow rate across the jump, and conserve energy in either of the two layers to close the set of equations. Alternatively, a closed set of equations conserving vorticity and layer volume flow rate can be used to predict jumps. As shear increases, the physics of the jumps changes, and entrainment becomes important. The theories can be modified to allow entrainment and to indirectly account for continuous velocity profiles, producing solutions where the basic theories failed. These jumps are investigated to illuminate the changing physics as shear increases. Simulations show that the amount of entrainment is related to the square of the upstream shear in both two-dimensional (2D) and three-dimensional (3D) simulations. However, they also show that the two-layer approximation becomes increasingly inaccurate, and 2D and 3D simulations disagree, at very high shear values. Furthermore, super- to super-critical transitions are also possible at higher shear, and while they exhibit a more gradual transition than a hydraulic jump, they can be analyzed using the same framework. The simulation results also illustrate the changing structure, vorticity balance, mixing, and energetic properties of the jumps as the upstream shear increases.

DOI: 10.1103/PhysRevFluids.5.074803

I. INTRODUCTION TO HIGH-SHEAR JUMPS

Internal hydraulic jumps occur in many environmental flows, including peripheral channels such as Knight Inlet in British Columbia and Hood Canal in Washington, and connecting channels such as the Pre-Bosphorus in Turkey. They may also occur in the deep ocean [1] as well as in the atmosphere [2]. In some cases, particularly in connecting channels, these jumps can be approximated as two-layered due to the contrasting properties of the exchanging water sources. Vertical shear upstream of the jump may be generated by topography or due to the inherent nature of an exchange flow. To address these internal hydraulic jumps in two-layered flows with upstream shear, Ogden and Helfrich [3] considered the simplified theories for predicting the jump height that were described by Wood and Simpson [4] (WS theory), Klemp *et al.* [5] (KRS theory), and Borden and Meiburg [6] (VS theory) and extended the theories to include upstream shear. The WS and KRS theories conserve the total momentum flux and the layer-volume flow rate across the jump and assume energy is conserved in the upper (WS) or lower (KRS) layer to close the set of equations and predict the height of a jump. The VS theory provides jump predictions by conserving vorticity. However, when upstream shear is added to these theories, solutions can be found only for a limited range of shear values. This work addresses the changing physics of the jump as shear increases beyond this range, and how the theories can be modified to account for these changes.

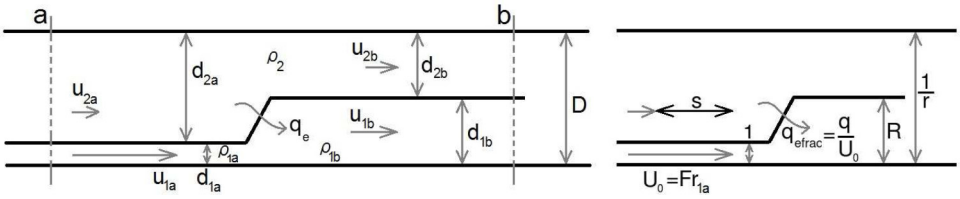

FIG. 1. Dimensional (left) and nondimensional (right) two-layer flow setup.

A two-layer hydraulic jump is shown in Fig. 1. The flow is analyzed in a frame of reference moving with the jump, so the jump speed is 0 and the flow is steady in time. Dimensionally, u is the layer velocity (relative to the jump), d is the layer depth, and ρ is the layer density. The subscript a (b) indicates upstream (downstream), and 1 (2) indicates the lower (upper) layer. D is the total depth, which in constant, and q_e is the volume flow rate of entrainment into the lower layer per unit width of the channel. Excluding entrainment, as in Ogden and Helfrich [3], the flow can be described by four nondimensional parameters: the lower layer upstream velocity $U_0 = \frac{u_{1a}}{\hat{U}}$, the upstream shear between layers $s = \frac{u_{1a}-u_{1b}}{\hat{U}}$, the total depth $r^{-1} = \frac{D}{d_{1a}}$, and the lower layer thickness downstream of the jump $R = \frac{d_{1b}}{d_{1a}}$. Velocities are nondimensionalized by $\hat{U} = \sqrt{g' d_{1a}}$ where $g' = \frac{g(\rho_1-\rho_2)}{\rho_1}$ is the reduced gravity, and the lengths are nondimensionalized by d_{1a}. In this setup and for the remainder of this work, the lower layer is assumed to be the expanding, or active, layer. The nondimensional setup including entrainment $q_{efrac} = \frac{q_e}{u_{1a} d_{1a}}$, which will be included in the modified theory, is depicted in Fig. 1. Given the upstream conditions U_0, s, and r, the downstream jump height R can be calculated using one of the basic theories [3].

Solutions to the WS theory are shown for shear values of $s = 0, 2, 5$, and 12 in Fig. 2. For shear values of $s \gtrsim 7$, with $r = 0.1$, and without entrainment or shape parameters that quantify the deviation from a two-layered flow, there are no longer mathematical solutions to the KRS, WS, or VS theories. Between shears of 2 and 5, the two solutions along $R = 1$ coalesce and then move off the $R = 1$ line. When this occurs, around $s \gtrsim 3$ for $r = 0.1$, there are no longer any allowable solutions, defined as having real phase speeds at the interface between the upper and lower layers, and conserving or dissipating energy across the jump. However, studies such as Wilkinson and Wood [7] have shown through experiments that jumps do occur with higher shear. This work investigates the physics of jumps as shear increases beyond the values allowed by basic two-layer theories. Previous work on high-shear jumps, which focuses on one-and-a-half layer flows with a stagnant upper layer, suggests that more mixing may occur and entrainment may be important. Holland *et al.* [8], Wilkinson and Wood [7], and Thorpe [9] include entrainment in their studies of high-shear jumps, and Thorpe [9] notes that for $U_0 > 7$ (with $s = U_0$ for a one-and-a-half-layer flows), entrainment is required for jump solutions to exist. This is consistent with the loss of solutions for the WS theory noted above. However, these studies considered one-and-a-half layer flows with a stagnant upper layer, while here, flows with two active layers are considered. Two-layer internal hydraulic jumps with large upstream shear are studied by adding entrainment to the two-layer theories investigated in Ogden and Helfrich [3]. The theory is compared to numerical simulations, and together, the physical mechanisms that change as upstream shear is increased are identified. The simulations further show that super- to supercritical transitions can also occur as shear increases, and the modified theory with entrainment is consistent with these simulations even though these transitions are not abrupt jumps.

Although most hydraulic jumps and transitions that occur in the environment have upstream shear values in the range considered in Ogden and Helfrich [3], it is important to understand how these jumps might change if the upstream conditions are altered [10–12]. Even modest dimensional shears could lead to the high-shear regime in weakly stratified flows. Furthermore, this work provides some insight into how localized hydraulic jumps and spatially developing shear flows are related.

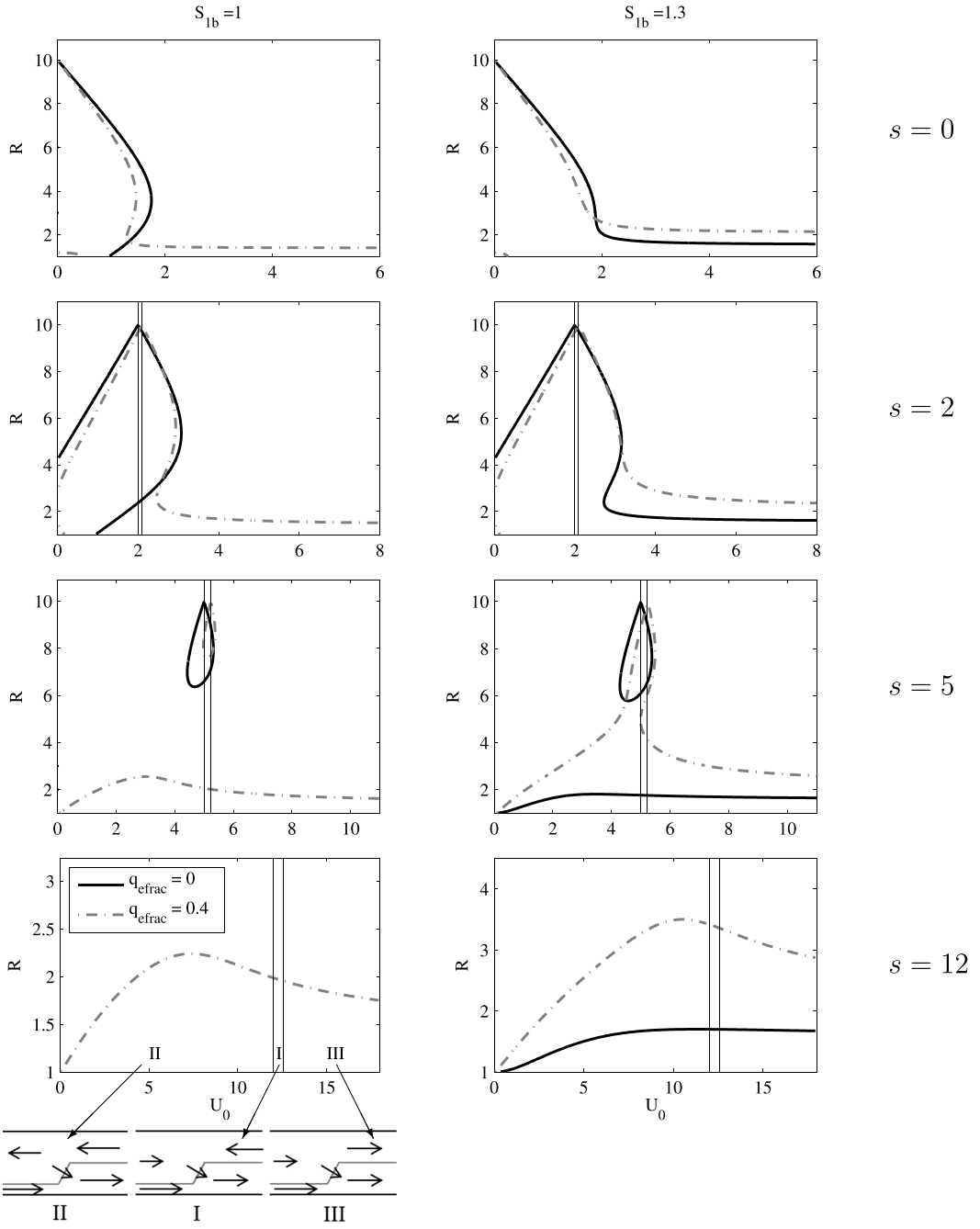

FIG. 2. Theoretical results with ($q_{efrac} = 0.4$, - - -) and without ($q_{efrac} = 0$, ——) entrainment. $S_{1a} = S_{2a} = S_{2b} = 1$. $S_{1b} = 1$ and 1.3 as indicated. $s = 0$, 2, 5, and 12, as indicated. Three regions of the solution space are identified based on the direction of the upper layer flow and are indicated in the lower left plot.

In Sec. II the two-layer theory with entrainment and shape parameters is developed. Section III describes numerical simulation results and shows how they compare to the theory. The comparison also suggests an approach for predicting the amount of entrainment. Section IV categorizes the structure, vorticity, and mixing properties of the jump.

II. TWO-LAYER THEORY WITH ENTRAINMENT AND SHAPE PARAMETERS

The two-layer theories discussed in Ogden and Helfrich [3] can be extended to include entrainment and shape parameters, which attempt to account for the continuous nature of the flow, particularly downstream of the jump. These modifications allow the theory to predict solutions at higher shear values. This approach is different from previous work that includes entrainment such as Wilkinson and Wood [7] and Holland *et al.* [8], who considered one-and-a-half-layer flows with stagnant upper layers. Here the total depth of the flow is limited, and the upper layer has a velocity that can be nonzero and different from the velocity in the lower layer. The theory is developed for an abrupt jump, although the results also describe super- to supercritical transitions, as discussed in Sec. III.

The flow setup is shown both dimensionally and nondimensionally in Fig. 1. The characteristic length scale is the upstream lower layer depth, d_{1a}, and $\sqrt{g' d_{1a}}$ is the velocity scale. These combine to give a timescale of $\sqrt{\frac{d_{1a}}{g'}}$. The only additional nondimensional parameter in the flow setup, compared to the low-shear flows described in Ogden and Helfrich [3], is the entrainment fraction,

$$q_{efrac} = \frac{q_e}{u_{1a} d_{1a}} = \frac{u_{1b} d_{1b} - u_{1a} d_{1a}}{u_{1a} d_{1a}}.$$

This is the fractional increase in the volume flow rate of the lower layer across the jump. The theory also allows nondimensional shape parameters, historically referred to as shape functions [7]. Shape parameters are not actually functions, but rather constants that attempt to account for departures from purely two-layered flow; they are nondimensional by definition and appear in the momentum flux equation (2.3), as described below.

Entrainment enters into the theory through the volume and mass conservation equations. The entrained fluid is assumed to mix completely throughout the entraining layer, instantaneously altering the layer's density across the jump. The entrainment is positive if the volume flow rate in the lower layer increases across the jump. The volume conservation equations with entrainment are

$$\begin{aligned} u_{1a} d_{1a} (1 + q_{efrac}) &= u_{1b} d_{1b}, \\ u_{2a} d_{2a} - q_{efrac} u_{1a} d_{1a} &= u_{2b} d_{2b}, \end{aligned} \tag{2.1}$$

where the subscript a (b) indicates the upstream (downstream) state. Because the density changes across the jump in the entraining layer, the lower (entraining) layer mass conservation equation,

$$u_{1a} d_{1a} (\rho_1 + \rho_2 q_{efrac}) = \rho_{1b} u_{1b} d_{1b}, \tag{2.2}$$

provides additional information. If the upper layer entrains fluid from the lower layer, the upper layer density would change across the jump, and the mass conservation equation for the upper layer would be of interest instead. Here the lower layer is always assumed to be the entraining layer, and this is consistent with the numerical simulations that are described in Sec. III.

The mass (2.2) and volume (2.1) conservation equations can be used together to obtain the density of the lower layer after the jump, given the entrainment fraction:

$$\rho_{1b} = \frac{\rho_1 + \rho_2 q_{efrac}}{1 + q_{efrac}}.$$

The entrainment does not alter the momentum flux conservation equation, except through the density, or $g' = g\frac{\rho_1-\rho_2}{\rho_1}$ in the Boussinesq approximation, which changes in the entraining layer across the jump.

The momentum equation will also be modified from the low-shear version by the inclusion of shape parameters. The momentum flux conservation equation is

$$\left[\int_0^D (p+\rho u^2)\,dz\right]_a^b = 0, \tag{2.3}$$

where the pressure is assumed to be hydrostatic away from the jump, and is given by

$$p(x, z = D) = p_s(x),$$

$$p = \begin{cases} p_s(x) + \rho_2 g(D-z) & d_1 \leqslant z \leqslant D \\ p_s(x) + \rho_2 g d_2 + \rho_1 g(d_1 - z) & 0 \leqslant z \leqslant d_1. \end{cases}$$

Here $[\cdot]_a^b$ indicates the difference between downstream and upstream.

Shape functions enter into the momentum flux equation (2.3) through the nonlinear terms. Shape functions for a continuous density profile could also be included in the hydrostatic pressure term and in the ρu^2 term of the momentum flux equation (2.3) [7]. However, the numerical simulations in Sec. III A show that the density profile usually remains approximately two-layered while the velocity profiles does not, so only shape parameters for the velocity profile are included here. The reason for the difference in profiles is discussed in Sec. III A. Furthermore, additional shape parameters would require specifying additional unknown parameters to predict a solution. With shape parameters for velocity only, and a constant density in each layer, the u^2 term in momentum flux equation (2.3) is

$$\int_0^D u^2\,dz = \int_0^{d_1} u^2\,dz + \int_{d_1}^D u^2\,dz.$$

Considering just the first term on the right-hand side, which is the flux in the lower layer,

$$\int_0^{d_1} u^2\,dz = \frac{\left(\int_0^{d_1} u\,dz\right)^2}{\left(\int_0^{d_1} u\,dz\right)^2}\int_0^{d_1} u^2 dz = \frac{u_1^2 d_1^2}{\left(\int_0^{d_1} u\,dz\right)^2}\int_0^{d_1} u^2\,dz = u_1^2 d_1 \frac{d_1\int_0^{d_1} u^2\,dz}{\left(\int_0^{d_1} u\,dz\right)^2},$$

where u_i is the layered average velocity,

$$u_1 = \frac{\int_0^{d_1} u\,dy}{d_1}, \quad u_2 = \frac{\int_{d_1}^D u\,dy}{d_2}.$$

Then, if shape parameters are defined as

$$S_1^2 = \frac{d_1\int_0^{d_1} u^2\,dz}{\left(\int_0^{d_1} u\,dy\right)^2}, \quad S_2^2 = \frac{d_2\int_{d_1}^D u^2\,dz}{\left(\int_{d_1}^D u\,dy\right)^2}, \tag{2.4}$$

the momentum flux equation (2.3) in the Boussinesq two-layer limit with shape parameters for the velocity profiles becomes

$$\left[\frac{p_s}{\rho_0}D + \frac{g'}{2}d_1^2 + S_1^2 u_1^2 d_1 + S_2^2 u_2^2 d_2\right]_a^b = 0. \tag{2.5}$$

Note that $\rho_{1a} = \rho_1(x=a) \neq \rho_1(x=b) = \rho_{1b}$, and $g'_b = \frac{g'_a}{1+q_{efrac}}$.

The shape parameters do not specify the shape of the velocity profiles, but simply attempt to quantify the deviation from a two-layered profile in a single number. Furthermore, using $S_1 = S_2 = 1$ will reduce the theory to the strictly two-layered limit.

As with the theories in Klemp *et al.* [5] and Wood and Simpson [4], a closure method must still be used to specify the change in surface pressure across the jump. Because fluid is being entrained from the upper layer into the lower layer and then mixed completely within the lower layer, energy cannot be conserved in the lower layer across the jump. Instead, following Wood and Simpson [4], energy is conserved along the upper streamline. This is consistent with Klemp *et al.* [5], who note that the Wood and Simpson [4] approach is appropriate for high-shear flows. Numerical simulations show that the approximation is usually good, with the change in $B = p + \rho gz + \rho\frac{u^2}{2}$ usually significantly smaller along the upper stream line than along the lower streamline. Conserving energy along the streamline at $z = D$ to get the change in surface pressure gives

$$\left[p + \rho_2 gz + \rho\frac{u^2}{2}\right]_a^b = 0.$$

Noting that ρgD is the same at sections a and b, and letting $p_s(x = a) = 0$, which is allowable because only the change in pressure across the jump is required, gives

$$p_s(x = b) = p_{sb} = \frac{\rho_2}{2}(u_{2a}^2 - u_{2b}^2).$$

Incorporating this result into the momentum flux equation (2.5) gives the following system of equations for a Boussinesq flow, which can be solved to fully specify the jump, if the entrainment, q_{efrac}, and the upstream and downstream shape parameters are known:

$$\frac{D}{2}(u_{2a}^2 - u_{2b}^2) + \left[\frac{g'}{2}d_1^2 + S_1^2u_1^2d_1 + S_2^2u_2^2d_2\right]_a^b = 0, \tag{2.6}$$

$$d_{2b} = D - d_{1b}, \tag{2.7}$$

$$u_{1b} = \frac{u_{1a}d_{1a}(1 + q_{efrac})}{d_{1b}}, \tag{2.8}$$

$$u_{2b} = \frac{u_{2a}d_{2a} - q_{efrac}u_{1a}d_{1a}}{D - d_{1b}}. \tag{2.9}$$

Shape parameters and entrainment could also be added to the vorticity conservation model, and an assumption for the surface pressure change across the jump would not be required. However, as shown in Sec. IV B, the turbulent vorticity divergence term becomes significant as shear increases in these flows, so the balance between mean vorticity divergence and mean baroclinic production of vorticity does not hold.

Nondimensional solution spaces of the two-layer theory with entrainment and shape parameters are shown in Fig. 2 for various shear values. In all cases, $S_{1a} = S_{2a} = S_{2b} = 1$. Results both with ($q_{efrac} = 0.4$) and without ($q_{efrac} = 0$) entrainment, and with $S_{1b} = 1.3$ and $S_{1b} = 1$, are shown for $r = 0.1$ so that the effect of adding these parameters is apparent. The basic two-layer theory ($q_{efrac} = 0$ and $S_{2b} = 1$, solid black curves in the left column) gives solutions for low shear values ($s = 0$ and $s = 2$). As shear increases to $s = 5$, a theoretical solution space exists, although wave speeds at the interface are complex, indicating that the solution may be unstable. This is also the range of shear values for which the solution space separates from the $R = 1$ line, as noted in Sec. I. The theoretical solution space disappears as shear increases to $s = 8$ and above. Adding entrainment of $q_{efrac} = 0.4$ to this theory (gray dashed line in left column) results in a theoretical solution space at all shear values. The shape of the solution space is also altered at low shear values. Instead of a limited range of U_0 values for which jumps exist, adding entrainment allows small jumps for unlimited values of U_0. As shear increases to $s = 5$, there are multiple solutions for a small range of $U_0 \approx 5$. The upper branches predict jump heights similar to the solutions without entrainment,

although real flows would likely produce jumps closer to the lower branch because energy loss is maximized on this branch of the curve. For larger shear values ($s = 12$), solutions exist only if entrainment is allowed, and jumps can occur for any shear value. This suggests that entrainment is important in jumps with larger upstream shear.

The solution space, with a shape parameter of $S_{1b} = 1.3$, is shown with and without entrainment in the right column of Fig. 2. Using this shape parameter gives solutions at all shear values shown, even without entrainment. This indicates that the two-layer approximation is less applicable as shear increases. However, previous work [7,8,13] indicates that entrainment is expected to be the most important physical difference between high- and low-shear jumps.

While the basic two-layer theory ceased to give solutions for shears of $s \gtrsim 7$, adding entrainment, shape parameters, or both results in a theoretical solutions space for much higher shear values. This implies that the governing physics changes as shear increases, and entrainment and continuous velocity profiles become necessary considerations. However, it should be noted that the value of the entrainment has been assumed, rather than calculated as part of the solution. The appropriate values of the shape parameters for a given flow are also unknown *a priori*.

In the solution space with entrainment, three regions exist that categorize the behavior of the upper layer of the flow. These are depicted in the lower-left panel of Fig. 2. In region II, an exchange flow occurs, with the upper layer everywhere moving in the opposite direction of the lower layer. In region III, the flow is unidirectional, with the upper and lower layer moving in the downstream direction, both upstream and downstream of the jump. In region I, the flow in the upper layer is toward the jump, both upstream and downstream of the jump. This region is only possible because the lower layer entrains fluid from the upper layer, while regions II and III exist for flows without entrainment. Region I spans a narrow range of U_0 values for typical values of entrainment. This work focuses on region III, so that fluid does not enter the computational domain through the outlet.

III. NUMERICAL SIMULATIONS

As with the two-layer theories without entrainment and shape parameters [3], this extended theory (2.6–2.9) neglects the dynamics within the jump or transition region and simply matches upstream and downstream states using momentum flux, mass, and volume conservation. However, hydraulic jumps and transitions can involve important nonhydrostatic effects in the jump head or transition region [3]. Therefore, numerical simulations are conducted to understand qualitative characteristics of the flows and to assess the validity of the two-layer theory. The simulations include continuous density and velocity profiles, although the upstream conditions are very close to two-layered, with a thin hyperbolic tangent interface for both density and velocity.

The numerical simulations are conducted using the CFD software Gerris [14]. The model solves the incompressible Navier-Stokes equations with the Boussinesq approximation,

$$\begin{aligned} \frac{\partial \vec{u}}{\partial t} + \vec{u}\cdot\nabla\vec{u} &= -\frac{1}{\rho_0}\nabla p + \nu\nabla^2\vec{u} - g\frac{\rho}{\rho_0}\hat{k}, \\ \frac{\partial \rho}{\partial t} + \vec{u}\cdot\nabla\rho &= \kappa\nabla^2\rho, \\ \nabla\cdot\vec{u} &= 0. \end{aligned} \tag{3.1}$$

The velocities are $\vec{u} = (u, v, w)$, where u is along channel, v is transverse [for three-dimensional (3D) simulations only], and w is in the vertical. The density deviation is ρ, p is the pressure deviation from hydrostatic, ν is the kinematic viscosity, κ is the density diffusivity, and $\hat{k}$ is the unit vector in the vertical direction. The simulations described here have no explicit viscosity or diffusivity, although they experience mixing due to the numerical scheme. The simulations are two-dimensional (2D) and have an isotropic grid with a resolution of 256 grid points in the vertical direction. Some 3D simulations were conducted, and these are described in Sec. V.

The numerical code uses the same basic advection algorithm as the IAMR model described in Ogden and Helfrich [3,15] and as such uses the implicit large eddy simulation (ILES) method of handling turbulence [14]. The ILES approach uses the numerical dissipation to represent the turbulent subgrid dissipation. In this case, a nonoscillatory, finite-volume Godunov scheme is used for the nonlinear advection terms, so that the leading order error term is in the form of a viscous stress tensor. This method has been successfully applied to unstratified turbulent flows [16–19], passive-scalar mixing [20], and stratified flows [21–23].

The Gerris code is used for these simulations because it allows topography through the use of mixed cells, which are cut by the boundary [14]. Downstream topography, similar to the setup in Wilkinson and Wood [7], and an inlet condition that changes in time [Eq. (3.3)] are included in these simulations to trigger an internal jump. This approach for developing a jump is taken here because the structure of the jump is unknown beforehand. Furthermore, the topography could affect the jump properties and may be used to make predictions about the jump, as discussed in Sec. III B. Without the topography and transient inlet condition, the upstream conditions could persist through the entire length of the domain. Topography also helps isolate the imperfect outlet boundary condition from the jump, reducing the effect of upstream-propagating disturbances on the jump. Finally, the topography could provide a constraint that helps determine the entrainment [7]. This approach is discussed further in Sec. III B. The topography used here has the form

$$h_T = \begin{cases} 0, & x < x_0 - c \\ h_{T,\max}\left(1 - \frac{(x-x_0)^2}{c^2}\right), & x_0 - c < x < x_0 + c \\ 0, & x_0 + c < x, \end{cases} \tag{3.2}$$

with $h_{T,\max} = 3$ unless otherwise noted, x_0 is typically 77 or 130, and $c = 22$.

The simulations are initialized with a layer of denser fluid with a depth equal to the desired upstream lower-layer depth. The density transitions to a lower value through a hyperbolic tangent profile,

$$\frac{\rho - \rho_{\min}}{\rho_{\max} - \rho_{\min}} = T = \frac{1}{2}\{1 - \tanh[\lambda(z-1)]\},$$

with $\lambda = 4.5$. This is shown in Fig. 3(a). The velocity field is initially stagnant throughout the domain. The inlet conditions on the upstream (left) side of the domain include a density profile matching the initial conditions within the domain. The inlet velocity ramps up smoothly from zero at the beginning of the simulation to the profile of the desired upstream conditions:

$$u(z,t) = \left(U_0 - s + s\frac{1}{2}\{1 - \tanh[\lambda(z-1)]\}\right)$$

$$\times\left\{H(t - 4\pi) + H(4\pi - t)\frac{1}{2}\left[1 + \cos\left(\frac{t}{4} + \pi\right)\right]\right\}, \tag{3.3}$$

where $H(\cdot)$ is the Heaviside function. The outlet boundary conditions are $\frac{\partial u}{\partial x} = \frac{\partial w}{\partial x} = \frac{\partial \rho}{\partial x} = 0$ and $p = 0$. This allows the fluid to leave the domain. If the barotropic flow is too slow, a bore will propagate into the domain along the upper boundary; however, the flows used in the simulations shown here are fast enough to avoid this problem. The topography also helps isolate the outlet boundary condition from the hydraulic jump upstream by transitioning the flow to supercritical just before the outlet.

As the inlet velocity increases, a disturbance forms, as shown in Fig. 3(b). The figure shows the instantaneous tracer (or scaled density) field, T, of a flow with $r = 0.1$, $s = 10.8$, and $U_0 = 11.5$ during the development of the jump, where the flow has been nondimensionalized in the same way as the theory. The disturbance propagates downstream and over the topography, eventually developing into a statistically steady flow with a hydraulic jump in the region of the initial disturbance. Both the

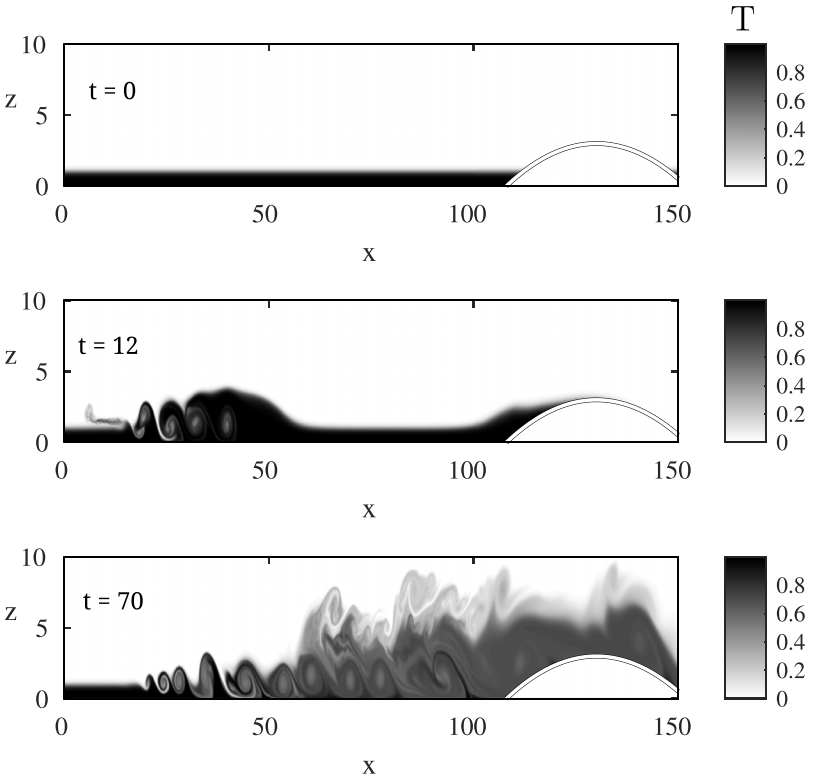

FIG. 3. Instantaneous scaled density field. Initial conditions ($t = 0$), development ($t = 12$), and fully developed flow ($t = 70$) are shown for a jump with $r = 0.1$, $s = 5.0$, and $U_0 = 5.6$. $R = 3.95$ and $q_{efrac} = 0.31$ are calculated from the simulation result.

pressure gradient due to this initialization and the bottom topography contribute to the development of the jump.

Due to the topography and the way the jump develops, the jump front is stationary, so the numerical results are naturally in the frame reference moving with the jump front. The upstream parameters U_0 and s are therefore defined at the inlet. By identifying the interface height using

$$\tilde{R}(x) = \int_0^{r^{-1}} T(x, z)\, dz, \tag{3.4}$$

a downstream average can be obtained using

$$R = \frac{\int_{x_2}^{x_1} \tilde{R}(x)\, dx}{x_2 - x_1},$$

where x_1 and x_2 are chosen to bound a downstream region in which $\tilde{R}(x)$ is approximately constant.

The entrainment is calculated from the numerical simulation using

$$q_{efrac} = \frac{\int_{x_1}^{x_2} \int_0^R u(x, z)\, dx}{x_2 - x_1} - \int_0^{\tilde{R}(0)} u(0, z)\, dz. \tag{3.5}$$

In this definition, the entrainment is the difference between the downstream and upstream averaged volume flow rates of the lower layer. For the example in Fig. 3, $R = 3.45$ and $q_{efrac} = 0.45$. The

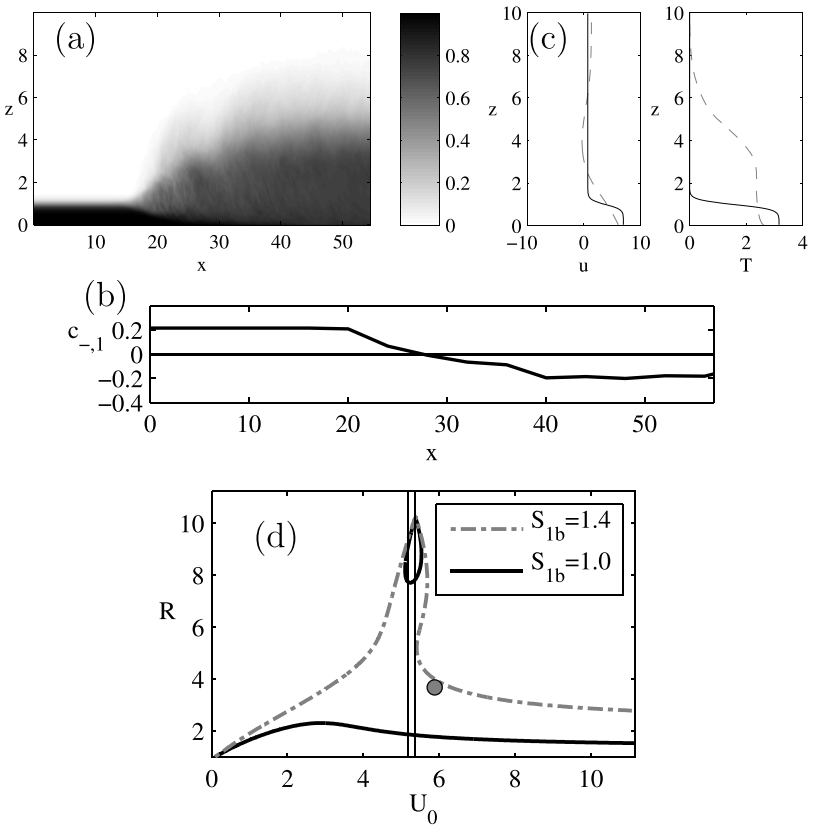

FIG. 4. Super- to subcritical transition with moderately high upstream shear. $r = 0.1$; $s = 5.1$; $U_0 = 5.9$; $R = 3.7$; $q_{efrac} = 0.34$, $S_{1a} = 1$, $S_{2a} = 1$, $S_{1b} = 1$, $S_{2b} = 1$. (a) Time-averaged tracer field of fully developed jump from $80 < t < 249$. (b) Phase speed of c_{1-}, the slowest moving wave, calculated using the continuous velocity and density profiles and the Taylor-Goldstein equation. (c) Upstream(___) and downstream (- - -) averaged velocity and density profiles. (d) Simulation result compared to theory, with entrainment in the theory set equal to the value calculated from the simulation and $S_{1a} = S_{2a} = S_{2b} = 1$. The simulation is indicated by the circle and the vertical lines separate regions II, I, and III, from left to right.

along channel points x_1 and x_2 define a downstream region after the jump, where the interface $\tilde{R}(x)$ is approximately constant in the along channel direction.

A. Simulation results

Simulation results confirm that super- to subcritical jumps occur at higher shear values than predicted by the basic two-layer theory, and that entrainment is substantial in these jumps. When the values for the entrainment and shape parameters used in the theory are consistent with those calculated from the simulations, the simulation results agree well with the theory, indicating that entrainment is an important physical process in high-shear jumps.

An example jump with an upstream shear of $s = 5.1$ is shown in Fig. 4. Despite the large upstream shear, a jump occurs. The downstream profiles exhibit a velocity minimum, and in fact a flow reversal, at a height of $z \approx 4.5$, close to the region of the largest density gradient. This reversal results in a velocity profile that is closer to three-layered than two-layered. It also deviates from the unidirectional flow assumed in other theories such as by Thorpe [9]. Due to this deviation, shape

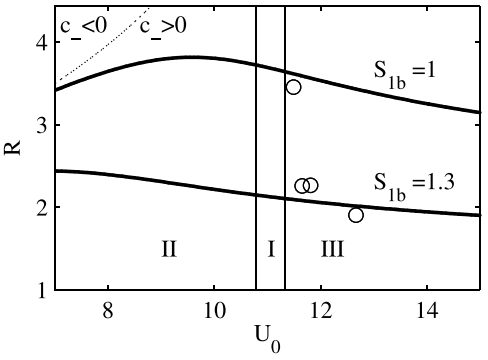

FIG. 5. Numerical results compared to theory for two sets of shape parameters, with $r = 0.1$, $s = 10.8$, and $q_{efrac} = 0.45$. $S_{1a} = S_{2a} = S_{2b} = 1$. In region II flow in the upper layer moves in the opposite direction from flow in the lower layer. In region I flow in the upper layer moves toward the jump, both upstream and downstream of the jump. In region III flow moves in the same direction as the lower layer, both upstream and downstream of the jump.

parameters are used in the theory to obtain reasonable agreement with the simulation. Figure 4(d) shows that the solution curve, using a constant entrainment of $q_{efrac} = 0.34$ calculated from (3.5), with shape parameters of $S_{1a} = S_{2a} = S_{2b} = 1$ and $S_{1b} = 1.4$, agrees fairly well with the simulation. The shape parameters calculated from the simulation results are $S_{1a} = 1.1$, $S_{2a} = 1.3$, $S_{1b} = 1.9$, and $S_{2b} = 1.9$, although the lower layer downstream parameter is the most important to consider because the lower layer velocities are larger. The values from this simulation show that the flow is deviating from two-layered in a non-negligible way.

The lower layer in the downstream density profile extends vertically to $y \approx 3.7$, while the velocity profile experiences a reversal from about $y \approx 2$ to $y \approx 6$. The flow reversal is due to recirculation in the lee of the jump, which creates a velocity profile that appears to have three layers, while the density profile appears two-layered. The recirculation mixes dense fluid up into the lower half of the middle layer of the velocity profile, and light fluid from the top of the domain into the upper half of the middle layer. In the two-layer approximation, the interface could therefore be identified as the velocity minimum, rather than where $u = 0$, which coincides much closer to the density interface. Ogden and Helfrich [3] showed in their Fig. 9(a) that for low-shear jumps of $s = 1$, there is no recirculation zone, and the velocity and density profiles are two-layered with a coincident interface, while for $s = 1.5$, a low-velocity region within the lower layer forms. Therefore, the transition from two-layered flows to those seen here begins at very low shear values.

Increasing the upstream velocity with a constant shear between the two layers results in a super- to supercritical transition similar to an expanding shear layer, rather than a hydraulic jump. This flow phenomenon can also be described using the same shock joining theory with entrainment, and shape functions closer to 1 than the super- to subcritical hydraulic jumps. Examples of such simulations are shown in the solution space in Fig. 5.

The simulations are compared to a solution curve with $S_{1a} = S_{2a} = S_{1b} = S_{2b} = 1$. The three simulations with larger U_0, which are all super- to supercritical transitions, fall near the theory. Figure 5 also shows the theoretical curve with $S_{1a} = S_{2a} = S_{2b} = 1$ and $S_{1b} = 1.3$. This theoretical curve is close to the simulation with the smallest value of U_0, which is a super- to subcritical jump. Both solution curves use $q_{efrac} = 0.45$. Although the actual values of entrainment vary between the simulations ($q_{efrac} = 0.36, 0.35, 0.41, 0.45$), all are reasonably close to this value. These results again show that for super- to subcritical transitions, the continuous downstream velocity profile must be accounted for in the theory, here by the use of $S_{1b} > 1$, to obtain agreement with the simulation results.

Figure 5 also shows the downstream criticality of the two-layered flow, with all shape parameters set to one, calculated using the two-layer phase speeds [24],

$$c_{\pm} = \frac{u_1 d_2 + u_2 d_1}{D} \pm \left\{ g' \frac{d_1 d_2}{D} \left[1 - \frac{(u_1 - u_2)^2}{g' D} \right] \right\}^{1/2}, \tag{3.6}$$

evaluated at b. In two-layer flows, only exchange flows, which occur in region I, exhibit subcritical flow downstream of the jump. However, some simulations in region III, where both layers flow in the downstream direction, are actually subcritical according to the internal long, linear wave speeds calculated from the Taylor-Goldstein equation [25] using the averaged continuous velocity and density profiles. This indicates that the shape of the continuous velocity profile can have important effects on the hydraulic state of the flow, which are not captured in the two-layer approximation.

Furthermore, simulations show super- to supercritical transitions can also occur, and these transitions can be predicted by the same shock theory with entrainment. For these high shear values, entrainment is significant in both jump types, indicating that it is an important physical process in high-shear jumps.

B. Predicting entrainment

The theory derived in Sec. II requires specifying the amount of entrainment into the lower layer. However, the entrainment depends on the upstream and jump parameters and should be part of the solution. Models for the amount of entrainment have been developed, for example, by Wilkinson and Wood [7] and Holland *et al.* [8], whose approaches are described here, and Thorpe [9] and Milewski and Tabak [26]. Thorpe [9] considers a continuously stratified flow under an infinitely deep, stagnant layer, and finds that entrainment is necessary for flows with $U_0 \gtrsim 7$, with $s = U_0$, in a two-layer flow. He finds a range of possible solutions with varying entrainment, and the actual solution depends on the upstream flow, the assumed structure of the downstream flow, and the specified entrainment.

Milewski and Tabak [26] conserve energy instead of layer volume, allowing the energy that would be lost across the jump to mix fluid between layers. They include an adjustable parameter that determines the efficiency of mixing. The Holland *et al.* [8] and Wilkinson and Wood [7] ideas, which apply to one-and-a-half-layer flows and build on the same shock joining theories that were explored in Ogden and Helfrich [3], are discussed here, and the Holland *et al.* [8] approach is extended to two-layer flows and compared to numerical simulations. A modified version of this approach is found to describe the entrainment reasonably well.

Holland *et al.* [8] consider the lower layer, depth-integrated energy flux in a reduced gravity, one-and-a-half-layer model, which, nondimensionally is

$$\left[\frac{d_1 u_1^3}{2} + b_g d_1^2 u_1 + d_1 u_1 e \right]_a^b = 0, \tag{3.7}$$

where e is the internal energy and b_g is the scaled density,

$$b_g = \frac{\rho - \rho_2}{\rho_2}. \tag{3.8}$$

They conserve energy across the jump by assuming that the turbulent energy produced within the jump is converted to internal energy, e. They then assume that the internal energy is related to turbulent kinetic energy through

$$e = d \left(\frac{1}{d_1} \int_0^{d_1} \frac{1}{2} < w^2 > dz \right); \quad < w^2 > \leqslant b_g z. \tag{3.9}$$

The upper limit on $< w^2 >$ exists because the buoyancy of the lower layer limits the production of turbulent kinetic energy. If more turbulent kinetic energy were produced, the energetic fluid would

mix up higher into the water column, and the layer would be thicker. Therefore, the maximum internal energy is

$$e = \frac{d}{4}(b_g h), \tag{3.10}$$

where d is a constant. In their work on one-and-a-half-layer flows with a stagnant upper layer, Holland *et al.* [8] attribute d to the number of dimensions of the flow, suggesting the value should be between 2 and 3. However, this work investigates the two-layer problem with an upper layer that has an independent velocity. Therefore, the upstream shear should affect the entrainment, possibly through the constant d.

Noting that, through the mass and momentum conservation equations,

$$u_{1b} = \frac{u_{1a} d_{1a}(1 + q_{efrac})}{d_{1b}}, \tag{3.11}$$

$$\rho_{1b} = \frac{\rho_1 + \rho_2 q_{efrac}}{1 + q_{efrac}}, \tag{3.12}$$

the entrainment, q_{efrac}, can be calculated using (3.7), (3.10), and (3.8) in terms of the upstream parameters and the one unknown, d_{1b}, or, nondimensionally, R. The limit of e, given by (3.10) is used instead of finding a general expression for $q_{efrac}(e)$ because e depends on b_g (3.10), which depends on ρ_{1b} (3.8), which depends on q_{efrac} (3.12). If internal energy from turbulence is allowed both upstream and downstream of the jump, the entrainment is given by

$$q_{efrac} = \left(\frac{d_{1b}^2}{d_{1a}^2} \left\{ 1 + \frac{2g}{u_{1a}^2} \left(1 + \frac{d}{4} \right) (d_{1a} - d_{1b}) \left(\frac{\rho_1}{\rho_2} - 1 \right) \right] \right\}^{\frac{1}{3}} - 1. \tag{3.13}$$

So far, this is simply the Holland *et al.* [8] approach applied to the lower layer of a two-layer flow. However, rather than calculating the entrainment from the jump height and a set value of d, the value of the constant d can instead be determined (in nondimensional parameters) using the jump height and entrainment from simulation results. This is given by

$$d = \frac{2U_0^2}{1 - R} \left[\frac{1}{R^2} \left(q_{efrac} + 1 \right)^3 - 1 \right] - 4. \tag{3.14}$$

Similar expressions can be found if turbulent energy is included only downstream of the jump:

$$q_{efrac} = \left(R^2 \left\{ 1 + \frac{2}{U_0^2} \left[1 - R \left(\frac{d}{4} + 1 \right) \right] \right\} \right)^{\frac{1}{3}} - 1 \tag{3.15}$$

and

$$d = \frac{4}{R} \left\{ 1 - \frac{U_0^2}{2R^2} \left[\left(q_{efrac} + 1 \right)^3 - R^2 \right] \right\} - 4. \tag{3.16}$$

This is reasonable for the flows with a laminar upstream studied here.

Figure 6 shows d versus s for a set of simulations. When the internal energy is included both upstream and downstream, the super- to supercritical 2D simulations diverge from the super- to subcritical 2D simulations as shear increases [Fig. 6(a)]. However, when the turbulence-related internal energy is included downstream but not upstream, all of the simulations collapse to a single curve, $d \approx 0.45 s^2$ [Fig. 6(b)], implying that the upstream shear is a controlling factor in the amount of entrainment. This modified Holland approach for q_{efrac} from (3.15) with $d = 0.45 s^2$ can be used in the two-layer theory (2.6)–2.9), giving a closed system for a given S_{1b}. For 3D simulations, $d \sim\propto s^2$, although the proportionality constant is different for super- to supercritical transitions, as shown in Fig. 6(c).

All simulations, including 2D and 3D super- to subcritical jumps and super- to supercritical transitions have entrainment controlled by s^2. Figure 7 shows that the entrainment and jump height

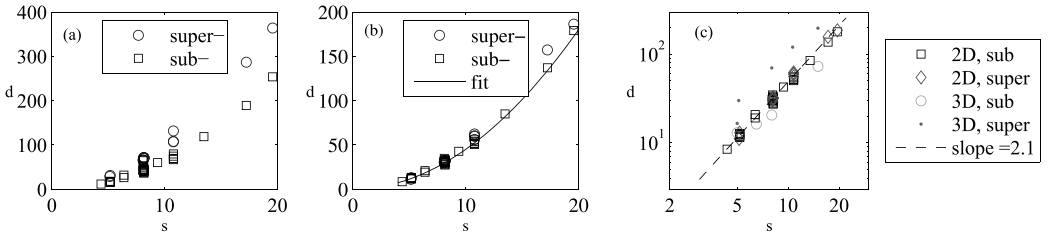

FIG. 6. Value of constant d versus shear s (a) with upstream turbulent energy and (b) without upstream turbulent energy, showing $d = 0.45s^2$ fit. (c) shows d vs s on a log-log scale for transitions with both super- and subcritical flow downstream, for 2D and 3D jumps.

predicted by the modified Holland theory with $d = Cs^2$ agrees well with the entrainment and jump height calculated from the numerical simulations if an appropriate shape parameter and constant C is used ($C = 0.45$ for 2D simulations and 3D super- to subcritical jumps). The shape parameters shown in Fig. 7 were used as fitting parameters and chosen so that the curves pass through the simulation points. The best value of S_{1b} for a given flow is not obvious *a priori*, and the theory is more sensitive to S_{1b} as U_0 increases. However, the shape parameters the best fit the theory to the simulations are similar to the values calculated from the simulations, indicating that shape parameters provide a reasonable physical description of the flow.

As the upstream shear increases, the flow begins to behave as an expanding shear layer; the entrainment is related to s^2 and is therefore also related to the gradient Richardson number, $\mathrm{Ri}_g = \frac{g' \frac{\partial T}{\partial z}}{T_1 (\frac{\partial u}{\partial z})^2}$. Furthermore, the jump region through which entrainment occurs is longer than the jump heads, where $\tilde{R}(x)$ [Eq. (3.4)] changes rapidly, found in the low-shear cases. The entrainment region extends in the along-channel direction until the mean gradient Richardson number at the interface is close to $\mathrm{Ri}_g = \frac{1}{4}$, and the flow becomes stable to Kelvin-Helmholtz instabilities. Figure 8 shows the gradient Richardson number along the interface for both low- and moderate-shear simulations. When $s = 1.5$ [Fig. 8(a)], the jump is abrupt with Ri_g dropping below $\frac{1}{4}$ through the jump. This flow also has negligible entrainment ($q_{efrac} < 0.1$). As the shear increases to $s = 5.1$, the entrainment increases ($q_{efrac} = 0.45$) and the length of the jump region, where $\tilde{R}(x)$ [Eq. (3.4)] changes rapidly, increases substantially, extending from $20 \lesssim x \lesssim 40$. The higher shear jump behaves as a slowly expanding shear layer rather than an abrupt transition as assumed. However, both of these flows can be analyzed as hydraulic jumps if this shear-controlled entrainment is included across the transition.

Other approaches to predicting the entrainment in a hydraulic jump include the work of Wilkinson and Wood [7], who consider a one-and-a-half-layer flow over an obstacle. They apply a

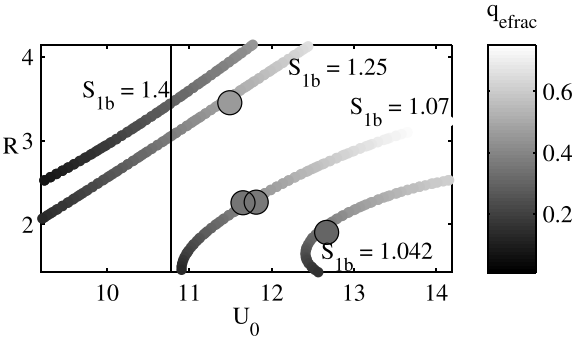

FIG. 7. Simulation and theory results for modified Holland *et al.* [8] model with turbulent energy downstream only. $s = 10.8$ and $r = 0.1$.

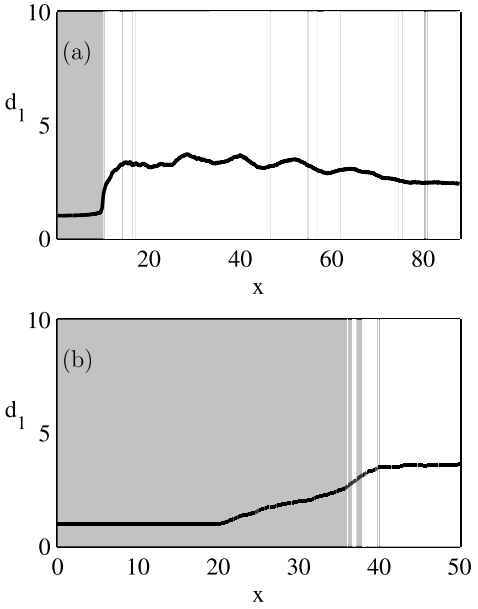

FIG. 8. Stability according to gradient Richardson number for flows with (a) $s = 1.5$, $U_0 = 2.6$ and (b) $s = 5.1$, $U_0 = 5.8$. $r = 0.1$. Gray indicates regions where $\mathrm{Ri}_g < 0.25$ at the interface (unstable), and white indicates regions where $\mathrm{Ri}_g > 0.25$ at the interface (stable). The solid line is the interface.

shock-joining approach across the jump, and then conserve energy between the region downstream of the jump and the crest of the sill, with the added constraint that the flow is critical over the sill. These requirements fully constrain the problem, and the entrainment is implicit in the solution. This method could be applied to the two-layer problem with upstream shear. However, numerical simulations show that the flow is not consistently controlled at the peak of the downstream topography, so accurate predictions were not found from this approach.

IV. JUMP PROPERTIES

The numerical simulations reveal how properties of the transitions change as the shear increases, in addition to allowing comparison with theoretical predictions. These properties are discussed in the following sections.

A. Structure of transitions

Wilkinson and Wood [7] described hydraulic jump structures in flows with deep, stagnant upper layers as having an entrainment region and a roller region, as sketched Fig. 9. In the entrainment region, fluid crosses the interface from the upper into the lower layer, and is assumed to mix throughout the lower layer. In the roller region, fluid recirculates at the interface. Regev and Hassid [13] also find these structures in numerical simulations of hydraulic jumps in one-and-a-half-layer flows with high upstream shear. The detailed structure of transitions in two-layered flows varies depending on the type of transition, as shown in the time-averaged, fully developed flows in Fig. 10. For super- to subcritical hydraulic jumps, an entrainment region exists at the leading edge of the jump, shown at $x \approx 20$ in Fig. 10(a). Downstream of the entrainment region are vortices that intersect the mean interface.

These are similar to the entrainment and roller regions first described by Wilkinson and Wood [7]. In a super- to supercritical transition, such as in Fig. 10(b), an entrainment region appears at

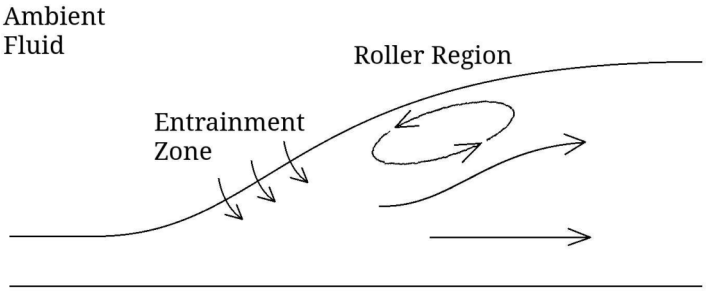

FIG. 9. Flow structure described by Wilkinson and Wood [7] for one-and-a-half-layer flows.

the head of the jump, although the roller region (or downstream vortices) is absent. Intermediate, or double, transitions also exist, in which there is a super- to supercritical transition followed by a super- to subcritical jump. An example is shown in Fig. 10(c), where the super- to supercritical transition occurs from $15 \lesssim x \lesssim 30$ and the super- to subcritical jump occurs for $30 \lesssim x \lesssim 50$. The intermediate transition can be compared to the theory as either a super- to supercritical transition with shape parameters of approximately one, where the region between $x = 30$–40 in Fig. 10(b) is considered the downstream region, or a super- to subcritical jump where $x = 45$–55 is the downstream region.

The type of transition that occurs depends primarily on $u_{2a} = U_0 - s$, and less so on h_T, the downstream sill height, as illustrated in Fig. 11. Flows with $u_{2a} = U_0 - s \lesssim 0.8$ tend to generate super- to subcritical jumps, whereas flows with larger $U_0 - s$ produce super- to supercritical transitions. The intermediate jump type exists for $U_0 - s \approx 0.8$ and $h_{T,\max} = 3$. For the same $U_0 - s$, shorter topography results in a super- to supercritical transition and larger topography produces a super- to subcritical jump. A double transition is plotted twice in Fig. 11, once as a super- to subcritical jump, which occurs from the upstream to final downstream state, and once as a super- to supercritical transition, which occurs from the upstream to intermediate states.

The Wilkinson and Wood [7] theory accounts for the weir height, requiring that the flow be critical at the crest of the weir, as discussed in Sec. III B. However, these two-layer flows can remain subcritical over the entire topography downstream of the jump, be controlled at the crest, be controlled upstream of the crest, or remain supercritical over the topography. Therefore, the precise height of the weir does not determine the jump properties, but instead groups solutions based on whether the flow transitions to subcritical across the jump, which occurs for higher weirs, or remains supercritical over the topography, which occurs for low weir heights.

The distance between the inlet and the weir can also impact the jump structure if the distance is small relative to the length of the entrainment and roller regions. In that case, the length of the entrainment region, and therefore the total entrainment, is reduced. In the simulations shown here, the distance to the weir is always long enough that increasing the distance does not affect the jump.

Wilkinson and Wood [7] conducted experiments of approximately one-and-a-half layer flows that produced hydraulic jumps. Their experiments included a fast moving active layer under a deeper ambient layer, which develops only a velocity through interaction with the lower layer. The simulations conducted here include actively forced, finite depth upper layers, with velocities of about 10%–15% of the velocity of the lower layer. Furthermore, the Wilkinson and Wood [7] experiments have a no-slip bottom, whereas the current simulations have a free-slip bottom boundary. Nonetheless, when the numerical results are compared to the experiments, the most significant differences that arise are reasonably explained by the differences in flow setup.

The density profiles of two simulated two-layer hydraulic jump are similar to Wilkinson and Wood's [7] experimental profiles (Wilkinson and Wood's Fig. 10), as shown in Fig. 12(a). In Fig. 12 the plotted variables are consistent with Wilkinson and Wood's: $\frac{z}{R}$ and $\frac{T}{\frac{q_\Delta}{q_L}}$, where $q_\Delta = \int_0^1 uT\, dz$

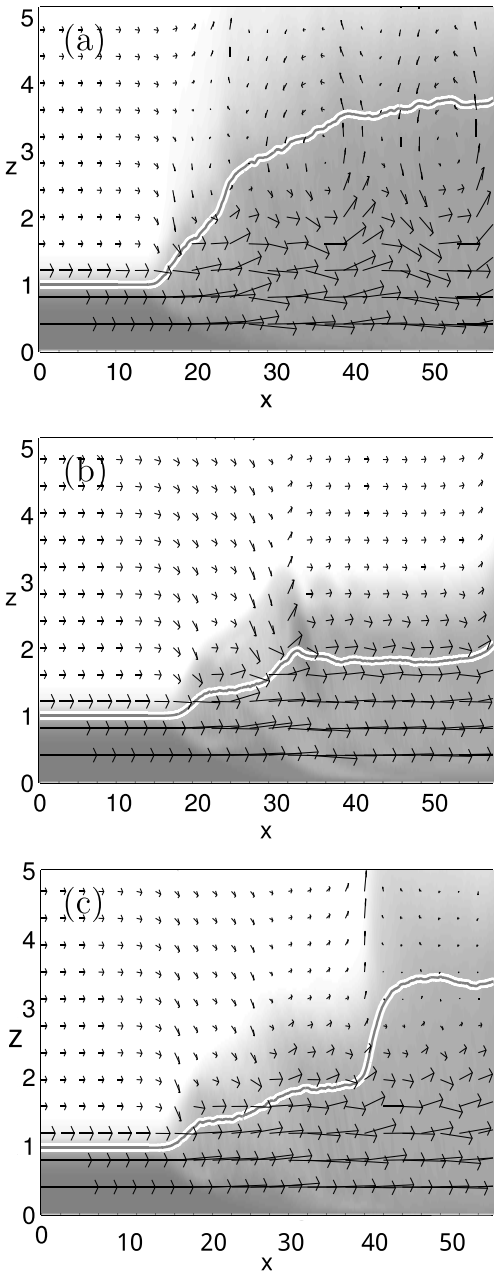

FIG. 10. Jump structures of (a) a super- to subcritical jump with $U_0 = 8.75$, (b) a super- to supercritical jump with $U_0 = 9.025$, and (c) a jump with a super- to super-critical transition followed by a transition to subcritical flow, with upstream $U_0 = 8.85$. In all cases, $s = 8$ and $r = 0.1$.

and $q_L = \int_0^R u\, dz$. The experimental profiles correspond to flows with an upstream $\mathrm{Fr} = \sqrt{\frac{q_L^3}{q_\triangle R}} = 7.1$ for partially and maximally entraining jumps. The extent of the entrainment in the experiments is determined by the length of the entraining zone, which is limited when the downstream Froude number reaches one. Because the upper layer in the simulations has a forced velocity at the inlet, this classification does not apply to the simulations; however, the simulations shown have lower

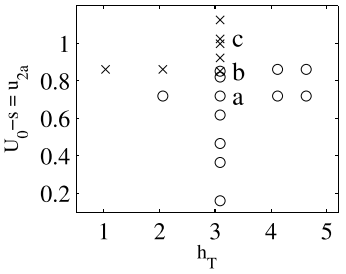

FIG. 11. Regime diagram of jump structures. Double jumps are included as both super- to super- and super- to subcritical transitions. x indicates super- to supercritical transitions, and $\circ$ indicates super- to subcritical transitions.

entrainment than the maximum values found across all simulations considered in this paper, as discussed in Sec. IV C. Both the partially and fully entraining experimental profiles are shown for comparison with the simulations. Two simulations with upstream Froude numbers of 5.6 and 6.7 are shown for comparison with the experimental results. These simulations are chosen because the upstream Froude number of 6.7 is similar to the experimental value, and because details of the case with $\mathrm{Fr}_a = 5.6$ are shown in Fig. 4; the flow in the two simulations is very similar.

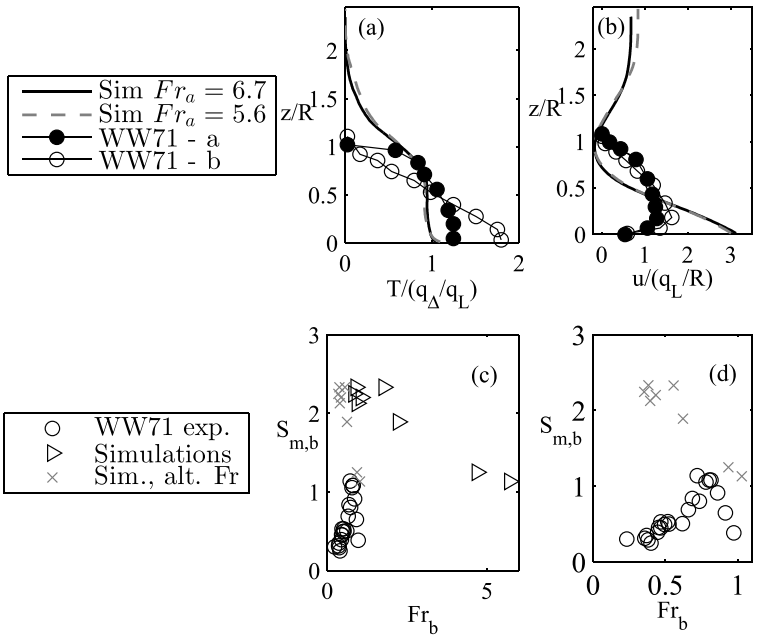

FIG. 12. Comparison between numerical simulations and Wilkinson and Wood [7] experiments. Simulation profiles of density (a) and velocity (b) are for a case with $\mathrm{Fr}_a = 5.6$, $r = 0.1$; $s = 5.1$; $U_0 = 5.9$; $R = 3.7$; $q_{efrac} = 0.34$, also shown in Fig. 4, and a case with $\mathrm{Fr}_a = 6.7$, $r = 0.1$; $s = 6.4$; $U_0 = 7.1$; $R = 3.8$; $q_{efrac} = 0.34$. The Wilkinson and Wood profiles are for partially (WW71-a) and maximally (WW71-b) entraining flows with $\mathrm{Fr}_a = 7.1$ from Fig. 10 in Ref. [7]. The momentum integral is plotted against the downstream Froude number in (c) and (d) (from Fig. 12 in Ref. [7]). An alternative $\mathrm{Fr} = \frac{u}{\overline{u} - c_{\min}}$, where $c_{\min}$ is the minimum wave speed calculated from the Taylor-Goldstein equation using the continuous velocity and density profiles, and $\overline{u} = r \int_0^{r^{-1}} u\, dz$.

The density profiles from the simulations suggest that the interface is higher than in the experiments, although the depth coordinate is nondimensionalized by the depth of the downstream interface for proper comparison to Wilkinson and Wood [7]. The apparently higher interface occurs because Wilkinson and Wood identify the interface as the height at which the velocity goes to zero, which is reasonable in their one-and-a-half layer flow. The interface of the simulated two-layer flow is identified as the height at which the vertical integral of the maximum density is equal to the total vertical integral of actual density, $\int_0^R dz = \int_0^1 T\, dz$, which is a more appropriate measure in flows that might not have a zero in the velocity profile. The stratification of the simulation in the region of the interface is similar to the stratification of the maximum entraining experiment of Wilkinson and Wood [7] (WW71-b).

The velocity profiles of the simulations [Fig. 12(b)] are different from the experiments (Wilkinson and Wood's Fig. 10 [7]) in a few important ways. The velocity at the bottom goes to zero in the experiments, while the simulation allows free-slip along the bottom. Second, the velocity in the upper layer of the simulations is forced to be larger than zero, whereas the experiments have an approximately stagnant upper layer. In the case of the simulations, this leads to entrainment of upper layer fluid with appreciable horizontal momentum and consequent changes in downstream flow structure. Given these distinctions precise agreement between the simulations and experiments is not expected.

A measure of the vertical integral of momentum through the lower layer, $S_m = \frac{\int_0^R u^2\, dz}{\frac{q_L^2}{R}}$, is compared to the downstream Froude number, $\mathrm{Fr} = \sqrt{\frac{q_L^3}{q_\Delta R}}$, for both Wilkinson and Wood's [7] experiments (Wilkinson and Wood's Fig. 12) and a set of simulations in Fig. 12(c). This comparison is closely related to the velocity profiles and allows a larger number of simulations to be compared. Downstream Froude numbers larger than one are included in the simulation results; one simulation corresponds to a super- to supercritical transition rather than an internal hydraulic jump. However, some correspond to internal hydraulic jumps and have negative wave speeds calculated from the Taylor-Goldstein equation using the average downstream velocity and density profiles. The simulations are also plotted using an alternative $\mathrm{Fr} = \frac{u}{\bar{u} - c_{\min}}$, where $c_{\min}$ is the minimum wave speed calculated from the Taylor-Goldstein equation using the average downstream density and velocity profiles. This correctly represents the flow's criticality. All of the numerical simulations exhibit larger downstream momentum than the experimental data. This is expected because the free-slip bottom boundary condition used in the simulations allows a larger velocity near the bottom, which contributes to the total momentum. Also, the interface in the experiments is identified as the height at which the velocity is zero. However, because the simulations with a forced upper layer do not necessarily have a velocity zero, the contribution to the momentum at and just below the interface is larger. The experimental setup of Wilkinson and Wood [7] differs from the two-layer flows investigated here in several significant ways. Despite these differences, the simulations are in qualitative agreement with the experiments, lending confidence to the model results.

B. Vorticity budget

Borden and Meibrug [6] develop a theory for predicting jump heights in flows without upstream shear, based on the conservation of mean vorticity. They integrate the vorticity equation over a domain extending through the depth of the flow, from upstream to downstream of the jump. The Reynolds-averaged vorticity budget integrated from the upstream position $x = 0$ to some downstream location x is

$$\left[\int_0^{\frac{1}{r}} \bar{u}\,\bar{\omega}_2\, dz\right]_0^x + \left[\int_0^{\frac{1}{r}} \overline{u'\omega_2'}\, dz\right]_0^x - \int_0^x \int_0^{\frac{1}{r}} \frac{\partial \bar{T}}{\partial x}\, dz\, dx = \left[\int_0^{\frac{1}{r}} \nu \frac{\partial \omega_2}{\partial x}\, dz\right]_0^x + \left[\int_0^x \nu \frac{\partial \omega_2}{\partial z}\, dx\right]_0^{\frac{1}{r}}. \tag{4.1}$$

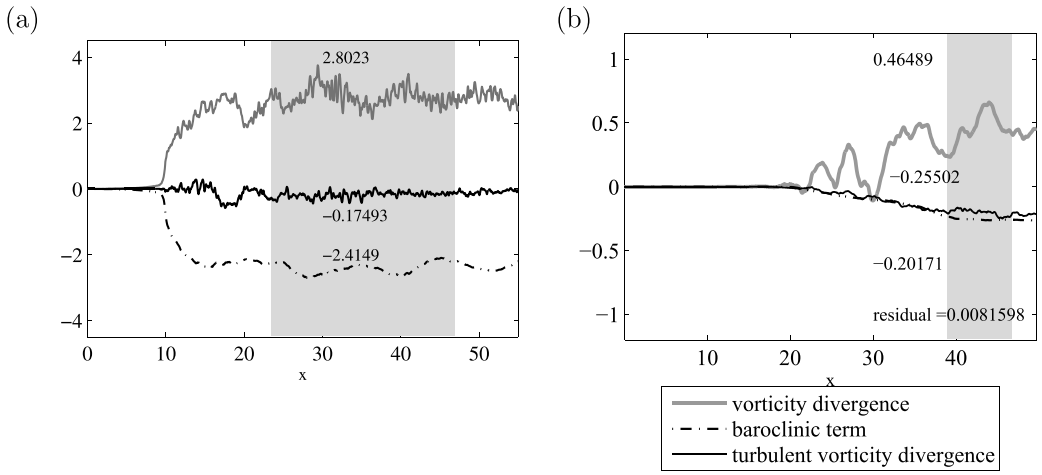

FIG. 13. Cumulative integral of the vorticity budget terms for jumps with (a) $r = 0.1$; $s = 1.5$; $U_0 = 2.59$; $R = 3.12$; $q_{efrac} = 0.078$ and (b) $r = 0.1$; $s = 5.2$; $U_0 = 5.9$; $R = 3.7$; $q_{efrac} = 0.34$. The value of each term, averaged through the gray region, is indicated.

Here $\vec{\omega} = \nabla \times \vec{u}$ is the vorticity, $\overline{(\cdot)}$ indicates a time average, and $(\cdot) = \overline{(\cdot)} + (\cdot)'$. The Borden and Meiburg [6] theory balances the mean baroclinic production (third term from the left) with the mean vorticity flux divergence (first term from the left), noting that diffusive losses [right-hand side of (4.1)] are negligible because vorticity is generated along the interface away from the boundaries [$\omega_{2,z}(z = 0, r^{-1}) \approx 0$] and does not vary in the along channel direction away from the jump [$\omega_{2,x}(x = a, b) \approx 0$]. Ogden and Helfrich [3] extend this idea to flows with small upstream shear, for which the same balance applies. However, as shear increases, the leading order balance of the vorticity budget changes. Due to the increasing upstream shear, turbulent advection of vorticity (second term from the left) becomes a more significant component, comparable to the baroclinic production of vorticity. The dominant vorticity budget balance begins to shift for jumps with shear in the transitional range of values ($3 \lesssim s \lesssim 7$) through which the theoretical solutions without entrainment are lost, as seen in Fig. 13, which shows the vorticity budgets for jumps with $s = 1.5$ and $s = 5.2$.

For 2D jumps with even larger shear, the leading balance is between the mean and turbulent vorticity flux terms and the residual, equal to the sum of the terms on the right-hand side of (4.1), remains small compared to the other terms in the balance, indicating that the budget has been resolved well and the ILES dissipation of vorticity is not significant. At these high shear values, the 2D simulation results also diverge from the 3D simulations. However, the leading order balance in the vorticity budget begins to change at moderate shear values at which the 2D and 3D results are still in agreement.

C. Trends in mixing efficiency and entrainment

As shear increases and entrainment becomes important, mixing efficiency through the jump, defined as the ratio of the downstream averaged cumulative buoyancy flux to the shear production,

$$\mathrm{Ri}_f = \frac{1}{b-a}\int_a^b \left(\frac{\int_a^b \int_0^{\frac{1}{r}} \overline{w'T'}\, dz\, dx}{\int_a^b \int_0^{\frac{1}{r}} \overline{u'w'}\frac{dU}{dz}\, dz\, dx} \right) dx,$$

decreases, as shown in Fig. 14. Although the buoyancy flux increases with shear, the shear production increases at a greater rate, resulting in a lower mixing efficiency. The decrease in mixing

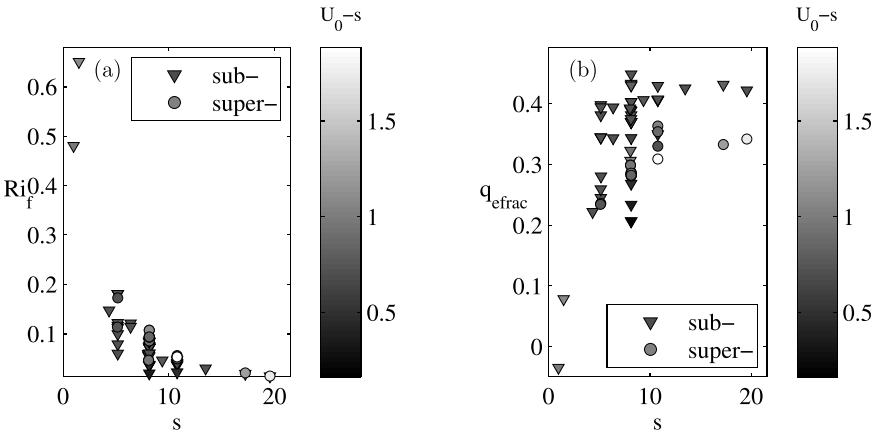

FIG. 14. (a) Mixing efficiency and (b) entrainment shown versus shear. Super- to supercritical and super- to subcritical jumps are identified by symbol type and $u_{2a} = U_0 - s$ is indicated by grayscale.

efficiency occurs through shear values of about $3 \lesssim s \lesssim 8$ for total depth of $D = r^{-1} = 10$. The entrainment increases through these shear values, from $q_{efrac} \approx 0$ for low shear flows, asymptoting to a value of $q_{efrac} \approx 0.4$ for larger shears [Fig. 14(b)]. The super- to subcritical jumps asymptote to a slightly higher entrainment than the super- to supercritical transitions. The transition region for both jump types occurs for $3 \lesssim s \lesssim 8$ and represents a transition from the abrupt, nonentraining ($q_{efrac} \approx 0$) hydraulic jumps described in Ogden and Helfrich [3] to a jump that behaves similarly to an expanding shear layer with mixing across the interface and, in these cases, significant entrainment. Although simulations of 2D and 3D transitions diverge at very high shear values, the trends in mixing efficiency and entrainment are apparent at moderate shear values ($s \lesssim 6$) at which the 2D and 3D simulations still agree.

V. COMPARISON WITH 3D CALCULATIONS

The numerical results shown so far are primarily from 2D simulations. In Ogden and Helfrich [3], 3D simulations of flows with low upstream shear were shown to behave similarly to the equivalent 2D flow, except in the mixing efficiency, which declined from $\mathrm{Ri}_f \approx 0.55$ for 2D simulations to $\mathrm{Ri}_f \approx 0.2$ for 3D cases. For larger shears, the 3D simulations begin to diverge from the 2D results, particularly for the super- to subcritical jumps. However, entrainment in the flows becomes significant for shear values of $s \gtrsim 4$ (with $r = 0.1$), and the differences between 2D and 3D simulations become prominent for higher shear values ($s \gtrsim 6$). Furthermore, the entrainment is related to s^2 in both 2D and 3D jumps, even as the shear increases significantly and the jumps become qualitatively different, as shown in Fig. 6. The trends in entrainment and mixing efficiency are also apparent at moderate shear values for which the 2D and 3D simulations agree. Therefore, the physical mechanisms discussed in this work are relevant to both 2D and 3D flows.

3D simulations were conducted using an isotropic grid with 128 grid points in the vertical, and the domain width is equal to the domain height. In 3D, as the shear increases, the mixed region begins to extend upward into the fluid until the dense fluid is mixed all the way up to the upper boundary, as illustrated in Fig. 15, which shows a super- to subcritical transition ($r = 0.1$ and $s = 5$, 6.5, and 8). In these high-shear flows ($s \gtrsim 8$), a large recirculating region develops near the upper boundary, just upstream of the sill. Figure 15 also shows velocity and tracer profiles upstream and downstream of the jump for each flow. As the shear increases, the flows transition from having a constant density upper layer, as seen in the lower shear jump [Fig. 15(a)], to having a continuous,

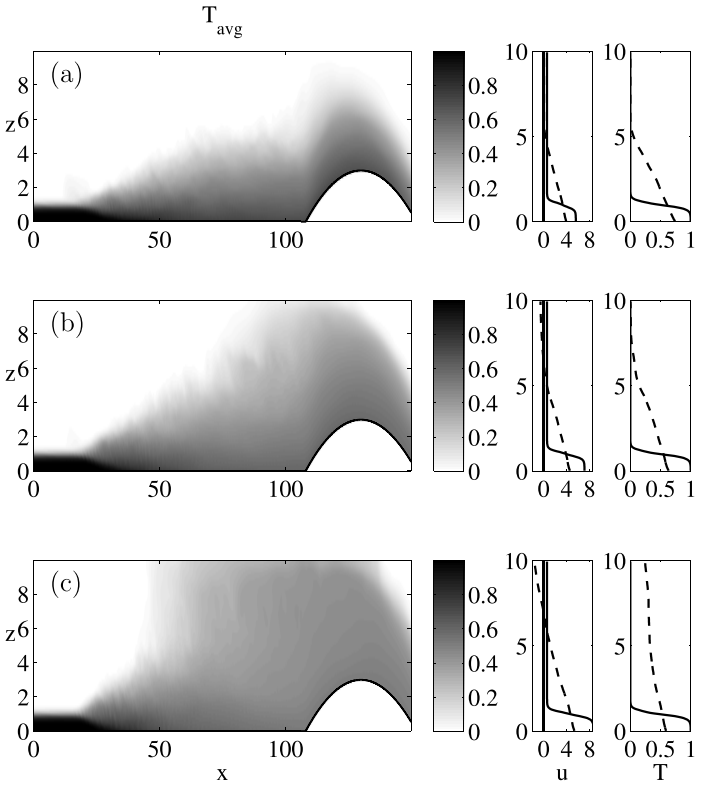

FIG. 15. Time-averaged 3D tracer field (left), upstream (——) and downstream (– – –) averaged tracer (T) and horizontal velocity (u) fields (right). (a) $s = 5$, $U_0 = 5.6$, (b) $s = 6.5$, $U_0 = 7.1$, and (c) $s = 8$, $U_0 = 8.6$. $r = 0.1$.

constant stratification throughout the depth [Fig. 15(b)], and then to having a well-mixed, constant density layer in the interior of the flow [Fig. 15(c)].

The difference between the 3D and 2D flows occurs because the coherent vortices of the 2D calculations break down with the introduction of transverse variations. This allows the fluid to mix more intensely [27]. Peltier and Caulfield [27] note that 3D mixing begins when 2D vortices reach their maximum amplitude, which, in these flows, appears to be limited by the lower layer depth. In 3D flows with very high shear, the density and velocity profiles deviate so significantly from two-layered that approximating them as such is unreasonable.

VI. CONCLUSIONS

Basic nonentraining two-layer theories for internal hydraulic jumps fail to provide solutions as the upstream shear increases. First, the allowable solutions, which require energy loss across the jump and real interfacial wave speeds, are lost. As shear increases further, even the nonphysical mathematical solutions cease to exist. However, previous work by Wilkinson and Wood [7], Thorpe [9], and Regev and Hassid [13] shows that hydraulic jumps in one-and-a-half layer flows with high upstream shear and a stagnant upper layer can exist. In the case of nominally two-layered flows with a nonzero upper layer velocity that is independent of the lower layer velocity, numerical simulations also result in jumps that, unlike the experiments of Wilkinson and Wood [7], are not controlled at the peak of downstream topography. Modifying the two-layer theory to include entrainment and/or shape parameters allows the theory to predict solutions for these higher shear flows. Entrainment

becomes important in the physics of the jump, for both super- to subcritical jumps and super- to supercritical transitions, and is required for the theory to be consistent with the simulations. Shape parameters improve the agreement between theory and simulations because they help account for the continuous velocity profiles; they are particularly important for super- to subcritical jumps with $U_0 - s = u_{2a} \lesssim 0.8$, while the values of the shape parameters are all very close to one for super- to supercritical transitions.

Various approaches to predicting the entrainment have been employed for one-and-a-half layer flows, such as the energy based approach of Holland *et al.* [8] and the flow control approach of Wilkinson and Wood [7]. The approach of Wilkinson and Wood [7] does not apply to the two-layer flows described here because the flow is not necessarily critical at the crest of the downstream topography. In this work, it is found that a modification of the Holland *et al.* [8] approach is consistent with the numerical simulations. Energy is conserved across the jump, and the energy dissipation in the jump is converted to internal energy to satisfy conservation. The energy dissipation is related to both the turbulent kinetic energy, as proposed by Holland *et al.* [8], and, through comparison with calculations, the square of the upstream shear. The relationship with the square of the upstream shear is a development for two-layered flows that was not proposed by Holland *et al.* [8]. This indicates that the upstream shear has a controlling influence on the amount of fluid that is entrained into the lower layer. As shear increases, the flow begins to behave similar to an expanding shear layer, although it can still be described as an entraining hydraulic jump. Significant entrainment is the primary physical difference between jumps with and without large upstream shear.

The modified theory can be improved by including shape parameters for the velocity profile because the profiles deviate significantly from a sharp two-layer flow. This indicates that the two-layer approximation becomes less appropriate as shear increases.

The numerical simulations show the range of flow structures that can occur for internal hydraulic jumps with large upstream shear and an active upper layer, which differs from the one-and-a-half layer high-shear flows studied previously [7]. These include super- to subcritical jumps, which have an entrainment and roller region similar to those described by Wilkinson and Wood [7] and Regev and Hassid [13], and super- to supercritical jumps, which exhibit an entrainment region but no roller region. These jump structures are very different from the jumps found in the low-shear flows of Ogden and Helfrich [3]. Furthermore, the jumps can be controlled at various points over, or not at all by, downstream topography.

The numerical simulations also show how the mixing efficiency in 2D is altered by increased upstream shear. There is a transition region between the low- and high-shear regimes, through which the entrainment increases from zero and the mixing efficiency decreases from about $\mathrm{Ri}_f \approx 0.55$. This transition region also occurs in the range of shear values where the theoretical solutions without entrainment lose the allowable and then theoretical solutions. For larger shear values, the entrainment asymptotes to about $q_{efrac} \approx 0.4$, with slightly larger values for the super- to subcritical jumps and slightly smaller values for the super- to supercritical transitions.

This work clarifies the changing physics of internal jumps and transitions as shear increases. The 2D and 3D simulations are similar for moderate shear values at which the physics begins to change ($4 < s < 7$), confirming that the extension of the 2D two-layer model to include entrainment is a reasonable approach since most of the results described carry over to 3D, such as the importance of entrainment, the jump structures, the changing vorticity balance, and the trends in mixing and entrainment for low to moderate shear. However, as shear increases further ($s > 7$), the 2D and 3D simulations diverge, particularly for super- to subcritical transitions. For this high-shear regime the flow can no longer be reasonably approximated with the 2D two-layer model and the 2D simulations are suspect. Nonetheless, it is noteworthy that the entrainment for both 2D and 3D jumps at all shear values depends on s^2.

Although most environmental flows in which the lower layer is of comparable depth to the upper layer generally have lower shear values in the range investigated in Ogden and Helfrich [3], an understanding of how the flows could change if the upstream conditions were modified

is important. Furthermore, due to the nondimensionalization, a flow with two layers that are very close in density effectively provides a high-shear flow. This work illustrates that as upstream shear increases, entrainment becomes a important physical process and the continuous velocity and density profiles become important, reducing, and perhaps eliminating, the applicability of the two-layered approximation.

ACKNOWLEDGMENT

This work was partially funded by Grant No. OCE-1029672 from the National Science Foundation.

[1] K. L. Polzin, K. G. Speer, J. M. Toole, and R. W. Schmitt, Intense mixing of Antarctic Bottom Water in the equatorial Atlantic Ocean, Nature (London) **380**, 54 (1996).
[2] D. K. Lilly, A severe downslope windstorm and aircraft turbulence event induced by a mountain wave, J. Atmos. Sci. **35**, 59 (1978).
[3] K. A. Ogden and K. R. Helfrich, Internal hydraulic jumps in two-layer flows with upstream shear, J. Fluid Mech. **789**, 64 (2016).
[4] I. R. Wood and J. E. Simpson, Jumps in layered miscible fluids, J. Fluid Mech. **140**, 329 (1984).
[5] J. B. Klemp, R. Rotunno, and W. C. Skamarock, On the propagation of internal bores, J. Fluid Mech. **331**, 81 (1997).
[6] Z. Borden and E. Meiburg, Circulation-based models for Boussinesq internal bores, J. Fluid Mech. **726**, R1-1 (2013).
[7] D. L. Wilkinson and I. R. Wood, A rapidly varying flow phenomenon a in two-layer flow, J. Fluid Mech. **47**, 241 (1971).
[8] D. M. Holland, R. R. Rosales, D. Stefanica, and E. G. Tabak, Internal hydraulic jumps and mixing in two-layer flows, J. Fluid Mech. **470**, 63 (2002).
[9] S. A. Thorpe, Turbulent hydraulic jumps in a stratified shear flow, J. Fluid Mech. **654**, 305 (2010).
[10] D. Farmer and L. Armi, Stratified flow over topography: The role of small-scale entrainment and mixing in flow establishment, Proc. R. Soc. London A **455**, 3221 (1999).
[11] M. C. Gregg and L. J. Pratt, Flow and hydraulics near the sill of Hood Canal, a strongly sheared, continuously stratified fjord, J. Phys. Oceanogr. **40**, 1087 (2010).
[12] M. C. Gregg and E. Özsoy, Flow, water mass changes, and hydraulics in the Bosphorus, J. Geophys. Res. **107**, 2-1 (2002).
[13] A. Regev and S. Hassid, On the streamwise development of density jumps, J. Fluid Eng. **132**, 021202-1 (2010).
[14] S. Popinet, Gerris: A tree-based adaptive solver for the incompressible Euler equations in complex geometries, J. Comput. Phys. **190**, 572 (2003).
[15] A. S. Almgren, J. B. Bell, P. Colella, L. H. Howell, and M. L. Welcome, A conservative adaptive projection method for the variable density incompressible Navier-Stokes equations, J. Comput. Phys. **142**, 1 (1998).
[16] L. G. Margolin, W. J. Rider, and F. F. Grinstein, Modeling turbulent flow with implicit LES, J. Turbulence, **7**, N15 (2006).
[17] F. F. Grinstein, L. G. Margolin, and W. J. Rider, editors, *Implicit Large Eddy Simulation: Computing Turbulent Fluid Dynamics* (Cambridge University Press, Cambridge, 2007).
[18] A. Aspden, N. Nikiforakis, S. Dalziel, and J. B. Bell, Analysis of implicit LES methods, Commun. Appl. Math. Comput. Sci. **3**, 103 (2008).
[19] Y. Zhou, F. F. Grinstein, A. J. Wachtor, and B. M. Haines, Estimating the effective Reynolds number in implicit large-eddy simulation, Phys. Rev. E **89**, 013303 (2014).
[20] S. Hickel, N. A. Adams, and N. N. Mansour, Implicit subgrid-scale modeling for large-eddy simulation of passive-scalar mixing, Phys. Fluids **19**, 095102 (2007).

[21] M. Waite and P. Smolarkiewicz, Instability and breakdown of a vertical vortex pair in a strongly stratified fluid, J. Fluid. Mech. **606**, 239 (2008).
[22] S. Remmler and S. Hickel, Direct and large eddy simulation of stratified turbulence, Int. J. Heat Fluid Flow **35**, 13 (2012).
[23] B. L. White and K. R. Helfrich, Rapid gravitational adjustment of horizontal shear flows, J. Fluid Mech. **721**, 86 (2013).
[24] P. G. Baines, *Topographic Effects in Stratified Flows* (Cambridge University Press, Cambridge, 2005).
[25] P. K. Kundu and I. M. Cohen, *Fluid Mechanics* 4th ed. (Academic Press, Amsterdam, 2008), p. 502.
[26] P. A. Milewski and E. G. Tabak, Conservation law modeling of entrainment in layered hydrostatic flows, J. Fluid Mech. **772**, 272 (2015).
[27] W. R. Peltier and C. P. Caulfield, Mixing efficiency in stratified shear flows, Annu. Rev. Fluid Mech. **35**, 135 (2003).